Earth, Planets and Space

FULL PAPER Open Access

Realization approach of non-linear postseismic deformation model for Taiwan semi-kinematic reference frame

Kwo-Hwa Chen[1], Ray Y. Chuang[2,3*] and Kuo-En Ching[4]

Abstract

Surface displacements associated with earthquake-cycle deformation of active faults significantly influence the accuracy of geodetic datum and reference frames, especially for the Taiwan area with high plate convergence and deformation rates. Following the current architecture of the semi-kinematic reference frame in Taiwan, which does not particularly consider the non-linear behavior of postseismic deformation, we explored the methods to implement a non-linear postseismic deformation model using the 2003 Chengkung earthquake as an example. Together with linear interseismic function, we utilized a logarithmic function to approximate the non-linear postseismic decays. For the time series without preseismic observations, we removed the interseismic velocities by spatial interpolation and fitted the resultant time series with the logarithmic function. After estimating postseismic decays for all GPS stations, we conducted two grid models of accumulative displacements for only postseismic deformation and total deformation after the earthquake. The first grid model provides a useful prediction for tracking surface movements, and the latter model provides a straightforward view to access the timing and amount of displacements to correct the semi-kinematic reference frame. The implementation of the grid models can well approximate non-linear postseismic trends for the semi-kinematic reference frame.

Keywords: Datum, Interseismic velocity, Coseismic displacement, Postseismic deformation

Introduction

The semi-kinematic reference frames implemented with surface deformation models are one practical approach to maintain the accuracy of reference frames distorted by the earthquake-cycle deformation. (Blick et al. 2003; Tanaka et al. 2007; Pearson et al. 2010; Pearson and Snay 2012; Blick and Donnelly 2016; Crook et al. 2016; Klein et al. 2019). Grid models of surface deformation used for the semi-kinematic reference frame usually contain interseismic velocities (e.g., McCaffrey 2005; Meade and Hager 2005; Ching and Chen 2015; Li et al. 2019) and coseismic displacements (e.g., Pearson and Snay 2012; Tanaka et al. 2007; Li et al. 2019). However, different from the signals of coseismic and interseismic deformation, the postseismic deformation shows transient, non-linear decay patterns (e.g., Shen et al. 1994; Savage and Svarc 1997; Freed et al. 2006). Afterslip and postseismic relaxation are two major mechanisms of postseismic deformation, which can be represented by logarithmic (Marone et al. 1991; Scholz 1998) and exponential (Nur and Mavko 1974; Pollitz 1997) functions, respectively. The two mechanisms may exist simultaneously and generate more complex decay patterns after large earthquakes (Hetland and Hager 2006; Tobita 2016). For most crustal faults, it is suitable to use one decay function to describe postseismic deformation (e.g., Hearn 2003; Savage et al. 2005; Freed et al. 2006). In terms of practically maintaining the reference frames, however, the methods to describe the postseismic decay pattern are nonunique. Many studies used the piecewise linear functions to approach the non-linear postseismic pattern (Altamimi et al. 2007, 2011;

*Correspondence: raychuang@ntu.edu.tw
[2] Department of Geography, National Taiwan University, Taipei 10617, Taiwan
Full list of author information is available at the end of the article

Blick and Donnelly 2016; Klein et al. 2019). Instead, some other studies used a ramp function (Crook et al. 2016) or proposed velocity varying with time after the earthquake (Li et al. 2019) to fit the non-linear trend. These linear functions can more or less correct the postseismic signals, but the fitting of these functions needs to wait until the non-linear decay is ceased or the complete postseismic deformation is finished. Therefore, a non-linear (logarithmic or exponential) function can describe the postseismic pattern appropriately (Bevis and Brown 2014) and this concept was used in the latest version of the International Terrestrial Reference Frame, ITRF2014 (Altamimi et al. 2016).

The island of Taiwan is located at a plate boundary zone with rapid deformation rates, causing the urgent need to maintain the reference frame. Since 1979, successive static reference frames were announced such as TWD67 (based on the GRS67 reference ellipsoid), TWD97 (based on the GRS80 reference ellipsoid with respect to ITRF94 at the epoch of 1997.0) (Yang et al. 2001), and TWD97[2010] (refer to ITRF94 at the epoch of 2010.0). Because the current TWD97[2010] datum was announced a decade ago with some major earthquakes occurred since then, a preliminary semi-kinematic reference frame was recently proposed and tested (Ching and Chen 2015; Li et al. 2019). Yet, these prior examinations did not particularly consider the non-linear postseismic decay. In addition, since the installation of continuously recorded GPS stations in Taiwan was conducted by different government agencies mainly including Academia Sinica, Ministry of Interior, Central Geological Surveys and Central Weather Bureau, the installation time of the GPS stations was diverse in a way that the stations were gradually installed after major earthquakes and the distribution of the most stations is not designed for specific faults (i.e., denser close to the faults and less dense away from the faults). Therefore, although current ~500 GPS stations in Taiwan provide a plausibly enough spatial density, the spatial and temporal resolutions of postseismic deformation around the seismogenic faults were generally insufficient.

Thus, to fully estimate the effects of earthquake-cycle deformation for accurately maintaining the reference frame in Taiwan, in the study we propose methods to characterize the non-linear postseismic deformation under the limitation of sparse spatiotemporal coverage. We used the 2003 Chengkung earthquake in eastern Taiwan as an example to examine the efficiency of non-linear function fitting and to explore the ways to utilize GPS data for correcting postseismic deformation without enough spatial and temporal resolution. With the consideration of the non-linear postseismic decay, the deformation models can more accurately characterize earthquake-cycle deformation and therefore assist the maintenance of semi-kinematic reference frames. Following the work of Ching and Chen (2015) and Li et al. (2019), this study focuses on the horizontal component only, which has a strong influence in cadastral surveys, and neglects the vertical component at the current stage of examination.

Tectonic background and the 2003 Chengkung earthquake

As an active arc-continental collision between the Eurasian and Philippine Sea plates (Suppe 1981, 1984; Teng 1990; Byrne et al. 2011) with a rapid plate convergence rate of 82 mm/year (Yu et al. 1997), the island of Taiwan is consequently having high deformation rates across active structures (Shyu et al. 2016) and high seismicity (Wu et al. 2008). The longitudinal Valley in eastern Taiwan is considered as the main suture zone between the Eurasian and Philippine Sea plates (Shyu et al. 2005). Two major active faults are present in the Longitudinal Valley: the Longitudinal Valley fault and the Central Range fault (Fig. 1). The Central Range fault is the west-dipping fault at the eastern side of the Central Range and became buried in the northern valley (Shyu et al. 2006), probably served as a retro-wedge fault (Chuang et al. 2014). The Longitudinal Valley fault located at the boundary between the western edge of the Coastal Range and the eastern edge of the valley has the highest geologic and geodetic fault slip rate in Taiwan (Chang et al. 2016; Ching et al. 2011; Shyu et al. 2016) and has partially ruptured during the 1951 Taitung–Hualien earthquake sequence (Shyu et al. 2007). The Longitudinal Valley fault has several segments (Shyu et al. 2005) and is partitioned into two strands to the southernmost end (Shyu et al. 2008; Chuang et al. 2012). In addition, the Longitudinal Valley fault in the southern half of the valley has significant fault creep (Lee et al. 2001, 2003; Hsu and Bürgmann 2006; Champenois et al. 2012).

The dense GPS network in Taiwan provides the information on surface deformation associated with the earthquake cycle (Yu et al. 1997; Hsu et al. 2009b; Lin et al. 2010; Ching et al. 2011). The M_w 6.8 Chengkung earthquake occurred in December, 2003 is the largest onshore earthquake after the 1999 M_w 7.6 Chi-Chi earthquake with a discernible postseismic deformation (Chen et al. 2006; Cheng et al. 2009). The earthquake occurred on the listric Chihshang reverse fault (Kuochen et al. 2007), which is one major segment of the Longitudinal Valley fault in the southern valley (Shyu et al. 2005). The coseismic fault slip is mainly concentrated at the depth between 5 and 20 km (Wu et al. 2006a; Ching et al. 2007; Hsu et al. 2009a). No shallow fault slip of the Chengkung earthquake and significant fault creep during the interseismic

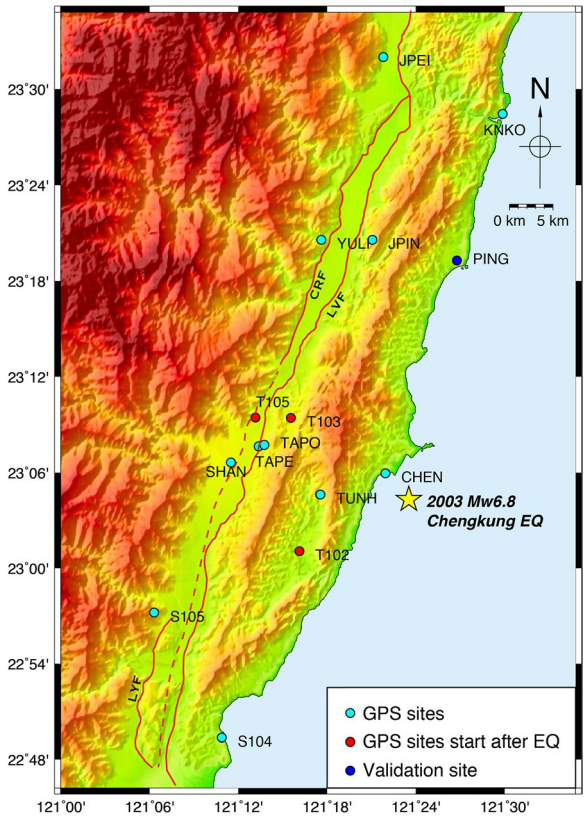

Fig. 1 GPS stations around the epicenter of the 2003 Chengkung earthquake (yellow star) used in this study. Cyan dots are GPS stations with complete time series and red dots are stations with only postseismic time series. Blue dot is the station used for validation of our grid model. Black vectors are interseismic velocities inferred from GPS time series fitting (for blue stations) or interpolated from surrounding stations (for red stations) with respect to ITRF2008. Red lines are active faults (Shyu et al. 2016). *LVF* longitudinal Valley fault, *CRF* Central Range fault, *LVF* Luyeh fault

period suggest the shallow portion of the Chihshang fault was less locked and had little strain accumulation. On the other hand, the deeper portion of the Chihshan fault was locked and capable for generating earthquakes. The postseismic deformation is mainly concentrated at the shallow depth (Cheng et al. 2009; Hsu et al. 2009a) and dominated by afterslip on the Chihshang fault (Perfettini and Avouac 2004; Savage and Yu 2007; Hsu et al. 2009a).

Postseismic deformation model of the semi-kinematic reference frame

To better characterize postseismic deformation for the maintenance of the Taiwan semi-kinematic reference frame, we examine the implementation of postseismic deformation models based on the concept of earthquake-cycle deformation. Particularly, we propose postseismic deformation models in the following three aspects: (1) when the GPS time series are sufficient to differentiate earthquake-cycle deformation (i.e., having interseismic, coseismic and postseismic signals), we examine the efficiency to generate a deformation model with a non-linear fitting function; (2) when GPS time series lacks pre-earthquake observations, the interseismic velocities are interpolated from surrounding stations to provide a basis for fitting non-linear postseismic decay; and (3) after the pattern of the postseismic decay at each station is fitted, we use a grid model to regionally estimate the amount of postseismic correction for the semi-kinematic reference frame. In the following sections, we presented the methods and results of these three aspects.

GPS time series data used in this study

We used GPS time-series data from the GPS Lab of the Taiwan Earthquake Center (http://gps.earth.sinica.edu.tw), which provides GPS daily solutions under the ITRF2008 (Altamimi et al. 2011). We selected 14 stations in the source are of the 2003 Chengkung earthquake for this study (Fig. 1). Eleven of 14 stations have observations of at least 2 years before and after the Chengkung earthquake. Six of 11 stations (KNKO, JPIN, CHEN, TUNH, TAPO and S104) are located in the hanging wall area (east of the Chihshang fault) and five stations (JPEI, YULI, TAPE, SHAN, S105) are in the footwall area (west of the Chihshang fault) (Fig. 1). The rest three stations located in the hanging wall (T102 and T103) and footwall area (T105) only have observations of less than 2 years with no preseismic data (Fig. 1). Because the M_w 6.1 Taitung earthquake occurred on April 1, 2006 (e.g., Wu et al. 2006b) around this region, which produced coseismic and postseismic signals at surrounding GPS stations, in this study we examined the postseismic deformation in the period between the 2003 Chengkung and 2006 Taitung earthquakes. Table 1 shows the information and observation periods of all the stations.

Non-linear postseismic fitting

Since we aimed to characterize the non-linear postseismic pattern, one fundamental basis is to isolate the trend of the different earthquake-cycle period. The most common approach is a mathematical fitting of GPS time series, also called trajectory models, with linear, step and non-linear functions for the interseismic, coseismic and postseismic periods, respectively (e.g., Nikolaidis 2002; Bevis and Brown 2014). Because afterslip is the major mechanism of the postseismic deformation of the Chengkung earthquake (Perfettini and Avouac 2004; Savage and Yu 2007; Hsu et al. 2009a), we chose a logarithmic function to describe the non-linear postseismic pattern

Table 1 Station information and data period

No.	Site ID.	Longitude (dd)	Latitude (dd)	Data period[a]	Antenna type	Note
1	JPEI	121.371	23.532	2002.05874–2019.15984	LEIAT504	Foot wall
2	S105	121.113	22.952	1993.00137–2019.15984	TRM14532.00	Foot wall
3	SHAN	121.200	23.109	2002.21995–2019.15984	LEIAT504	Foot wall
4	TAPE	121.231	23.126	2002.76366–2019.15984	LEIAT504	Foot wall
5	YULI	121.301	23.341	2001.96311–2010.91120	LEIAT504	Foot wall
6	CHEN	121.374	23.097	1994.03689–2019.15984	AOAD/M_T	Hanging wall
7	JPIN	121.359	23.341	2001.96585–2019.15984	LEIAT504	Hanging wall
8	KNKO	121.506	23.472	2002.30191–2019.15984	LEIAT504	Hanging wall
9	S104	121.189	22.821	1993.00137–2019.15984	TRM14532.00	Hanging wall
10	TAPO	121.237	23.127	2002.16257–2019.15984	LEIAT504	Hanging wall
11	TUNH	121.300	23.075	2002.30738–2019.15984	LEIAT504	Hanging wall
12	T102	121.277	23.016	2003.95219–2011.66257	LEIAT504	Hanging wall[b]
13	T103	121.267	23.155	2003.88388–2010.41393	LEIAT504	Hanging wall[b]
14	T105	121.227	23.156	2003.95219–2010.38388	LEIAT504	Foot wall[b]

[a] Chengkung and Taitung earthquakes are 2003.93852 and 2006.24454, respectively

[b] No preseismic data

(Marone et al. 1991; Scholz 1998). The fitting equation of the GPS time series is as below.

$$\begin{aligned} y(t_i) = {} & a + bt_i + c\mathrm{Cos}(2\pi t_i) + d\mathrm{Sin}(2\pi t_i) + e\mathrm{Cos}(4\pi t_i) \\ & + f\mathrm{Sin}(4\pi t_i) + \sum_{1}^{n_g} g_j H\left(t_i - t_{\mathrm{eq}}\right) \\ & + \sum_{1}^{n_h} h_j H\left(t_i - t_{\mathrm{eq}}\right) \cdot t_i \\ & + \sum_{1}^{n_k} k_j \cdot \log\left[1 + \left(t_i - t_{\mathrm{eq}}\right)/p\right] + \varepsilon \end{aligned} \tag{1}$$

where a is the initial coordinate and b is the steady interseismic velocity. c and d are the amplitude of annual variations, and e and f are the amplitude of semi-annual variations. g is the coefficient of step function H for permanent displacement, such as the antenna changes or coseismic displacements. h is the coefficient of the step function H for velocity change after the earthquake. k is the coefficient of the logarithmic decay and p is the characteristic time. ε is the residual between the observations y and fitting results. Because the characteristic time p could be different for each time series, we used a grid search method to select the optimal value of p for every time series. All the fitting time-series are available in Additional file 1.

To examine the efficiency and stability of the non-linear postseismic fitting with varied data lengths, we tested the fitting method with different postseismic data periods for every 30 days. For most crustal earthquakes without complex postseismic pattern, postseismic deformation can be characterized and fitted with a non-linear function. Conversely, the fitted non-linear function should be able to describe the non-linear postseismic pattern. Therefore, when the postseismic signals are well fitted, the fitted non-linear curve can predict further postseismic pattern if no significant coseismic jump occurs due to a large aftershock. Following this idea, we fitted GPS time series with postseismic observations every 30 days to examine monthly fitting results, and we then computed the root mean square (RMS) values between all fitting results and GPS data. Figure 2 shows two examples of 8 time-series fitting (30, 60, 90, 180, 360, 540, 720, and 840 days) at the stations SHAN and TAPO, which have significant postseismic deformation, and Fig. 3 shows the RMS results of the fitting curves. For the component with larger postseismic deformation (the east component of SHAN and the north component of TAPO), the logarithmic fitting of only 30-day data can predict future postseismic patterns well (Figs. 2 and 3). For the other component with minor postseismic deformation, the logarithmic fitting can better predict future postseismic pattern using data of at least 60 days (Figs. 2 and 3). There are some fluctuations of RMS values for the fitting with the time series of ~ 180–360 days (Fig. 3). This is probably because the fitting functions of semi-annual and annual variations have a strong influence in such a short time series.

In the current realization of the semi-kinematic reference frame in Taiwan, Li et al. (2019) fitted GPS time series with different linear velocities before and after an earthquake following the philosophy of piecewise linear fitting. Therefore, Li et al. (2019) practically incorporated

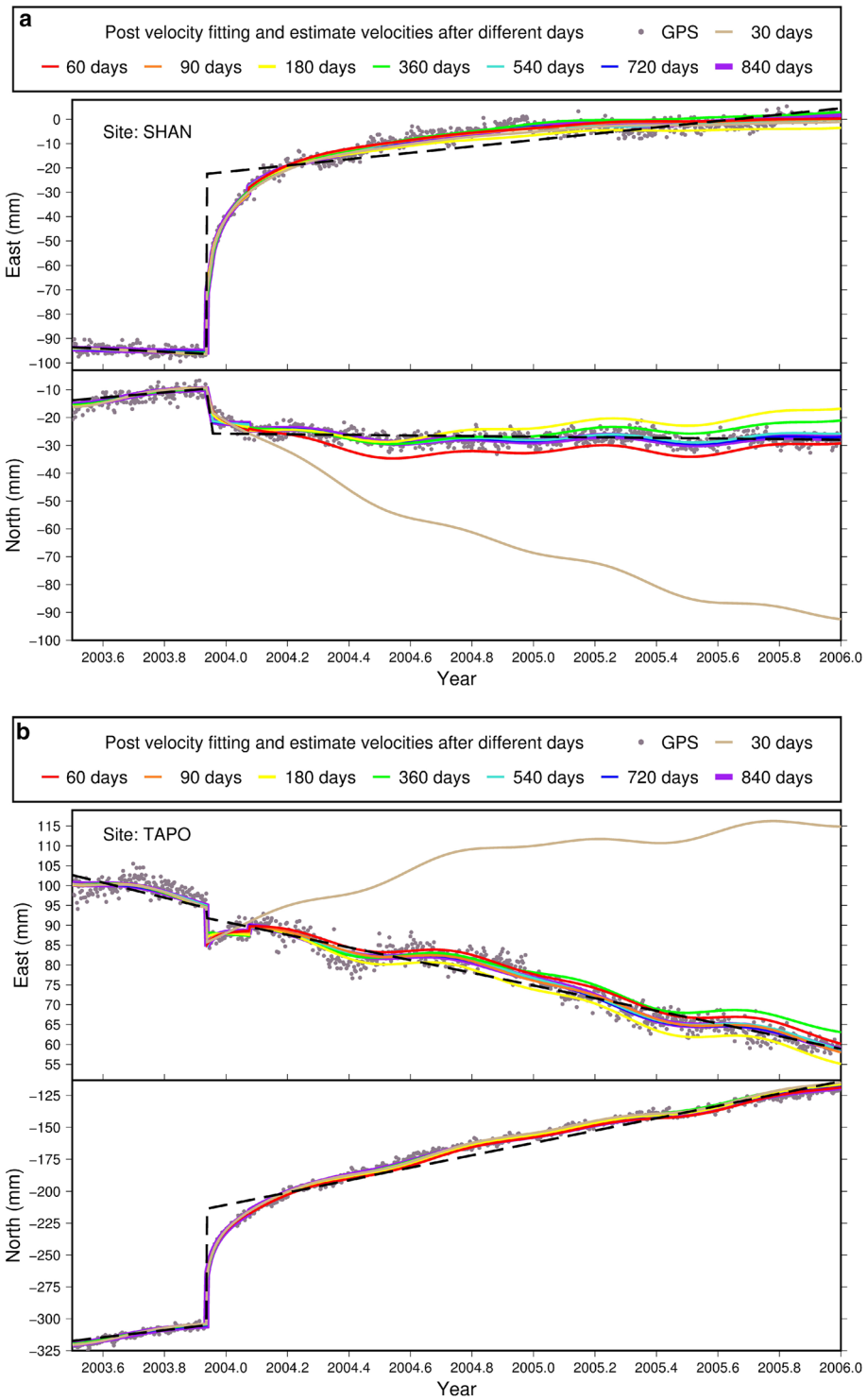

Fig. 2 Examples of GPS time series fitting for postseismic deformation at stations **a** SHAN and **b** TAPO. The time series were fitted with Eq. (1). All the time series have preseismic data for 2 years, but we only show preseismic data for half a year to focus on the postseismic fitting. Different color lines represent fitting curves derived from 30, 60, 90, 180, 360, 540, 720 and 840 days of data. Dash line is fitted by different linear velocities before and after the earthquake following the method of Li et al. (2019)

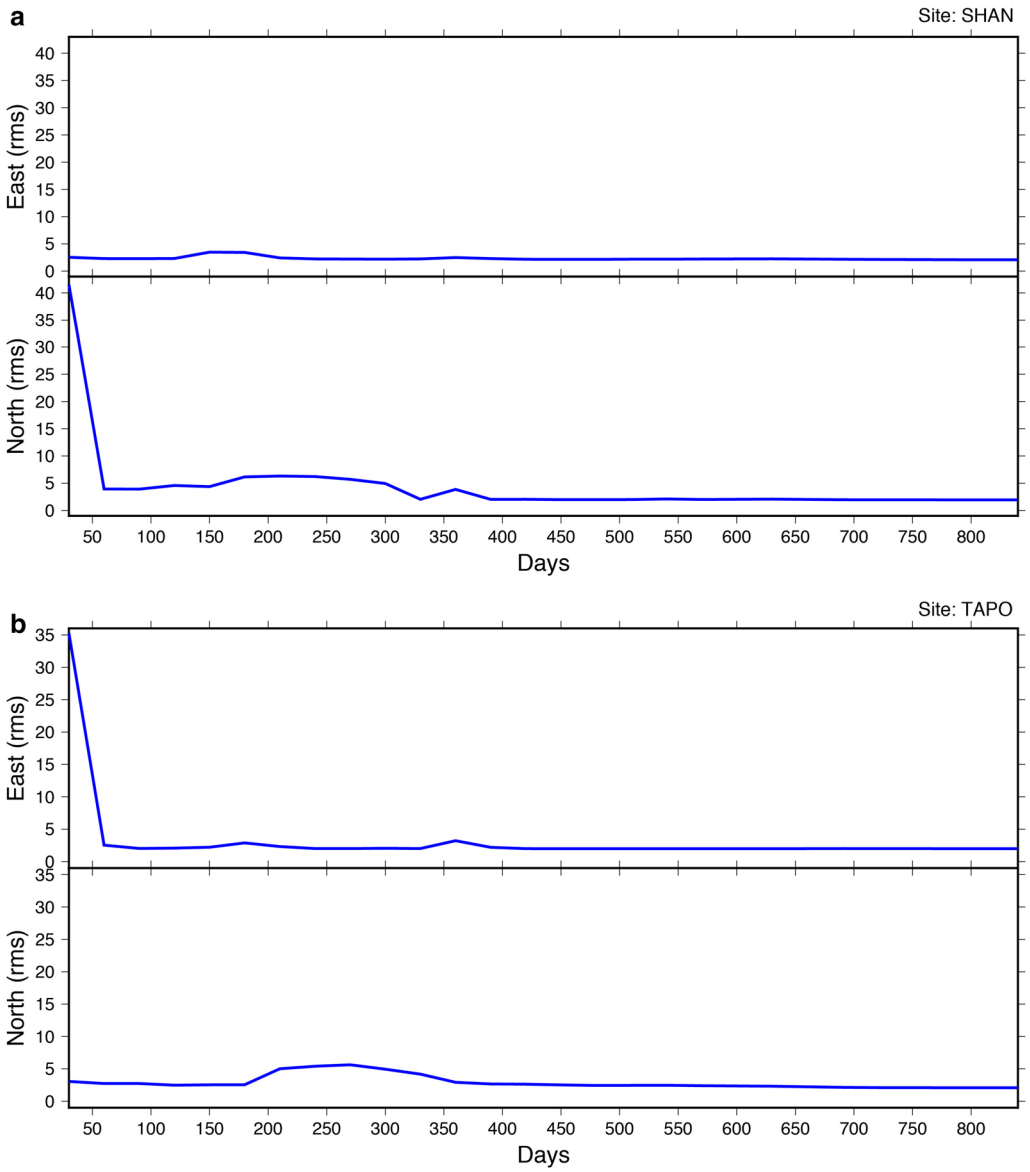

Fig. 3 RMS residuals between GPS data and predict data derived from fitting curves for every 30 days at stations **a** SHAN and **b** TAPO

postseismic deformation into interseismic deformation and did not particularly consider the non-linear postseismic deformation. To compare the results of Li et al. (2019) and our non-linear fitting, we used the first 60-day GPS results after the 2003 Chengkung earthquake, which is the time when our non-linear fitting starts to be effective as described above. We selected 5 GPS stations (CHEN, TUNH, TAPO, TAPE, and SHAN) closest to the epicenter, which have larger postseismic deformation. We computed the misfit for our non-linear fitting result and stepwise linear fitting result following the method of Li et al. (2019). The accuracy is 0.66 mm and 1.73 mm in the east and north components in our method, respectively. However, the accuracy is 4.12 mm and 5.58 mm in the east and north components using the piecewise linear fitting method, respectively. As the results, it shows that the improvement by our method is 70–80% than the method of Li et al. (2019).

Postseismic fitting for incomplete time series

The GPS installation may be conducted in response to postseismic observations after major earthquakes (e.g., Shen et al. 1994; Freed et al. 2006). However, it is more difficult to analyze the postseismic deformation from

Table 2 Interseismic velocities of all stations derived from time series fitting or interpolation

No.	Site ID.	Fitting Vn (mm/year)	Fitting Ve (mm/year)	Interpolated Vn (mm/year)	Interpolated Ve (mm/year)	Note
1	JPEI	17.51 ± 0.54	− 7.42 ± 0.46			Foot wall
2	S105	4.24 ± 0.54	− 3.46 ± 0.66			Foot wall
3	SHAN	9.45 ± 0.34	− 6.09 ± 0.32	8.51	− 6.34	Foot wall
4	TAPE	9.08 ± 0.44	− 10.05 ± 0.42			Foot wall
5	YULI	14.67 ± 0.46	− 6.50 ± 0.36			Foot wall
6	CHEN	33.02 ± 0.22	− 25.83 ± 0.18			Hanging wall
7	JPIN	32.46 ± 0.34	− 16.84 ± 0.30			Hanging wall
8	KNKO	31.96 ± 0.50	− 22.38 ± 0.42			Hanging wall
9	S104	29.30 ± 0.52	− 22.78 ± 0.62			Hanging wall
10	TAPO	27.13 ± 0.32	− 19.59 ± 0.30			Hanging wall
11	TUNH	23.35 ± 0.40	− 16.47 ± 0.54			Hanging wall
12	T102			25.11	− 18.30	Hanging wall[a]
13	T103			28.44	− 19.77	Hanging wall[a]
14	T105			9.79	− 7.51	Foot wall[a]

[a] No preseismic data

time series without preseismic observations. Although these stations do not have data before the earthquakes, they provide valuable observations of postseismic deformation that should be used to constrained reference frames. Nevertheless, direct fitting of only postseismic observations with the logarithmic and linear functions simultaneously might result in unrealistic results since the steady interseismic velocity cannot be well constrained by postseismic observations.

To better fit the logarithmic function for the time series without preseismic observations, we had to subtract interseismic velocities from the postseismic time series. Because the interseismic velocities result from steady fault creeping at depth, the pattern should be spatially correlated. For example, Yu and Kuo (2001) estimated interseismic velocities in eastern Taiwan, which is the area of this study, and showed that neighboring stations generally have velocities with similar movement directions if they are located at the same side of the fault (i.e., stations on the hanging wall are moving toward northwest while stations on the hanging wall have little motion with respect to the Central Range). Therefore, we interpolated the interseismic velocities for the stations installed after the earthquake from the velocities at the neighboring stations.

We first tested this method for the station with a complete time series to validate the method. We chose the station SHAN, which is located at the center of the study area in the footwall area, and estimated the interseismic velocity according to the surrounding stations also in the footwall area (JPEI, S105, TAPE, and YULI) using the linear interpolation. The interpolated velocities of 8.51 and − 6.34 mm/year are consistent with the velocities of 9.45 ± 0.34 and − 6.09 ± 0.32 mm/year derived from the time series fitting for the north and east components, respectively (Table 2). Thus, we were able to apply this method to the stations with incomplete time series.

We estimated interpolated velocities for the stations installed after the Chengkung earthquake and fitted the time series. We selected three stations (T102 and T103 on the hanging wall and T105 on the footwall) with apparent non-linear postseismic signals to examine the method for fitting incomplete time series. Since these three stations are in different sides of the fault, we interpolated velocities for the hanging wall and footwall, separately. We used the velocities derived from the fitting of the complete time series (Table 2) for the spatial interpolation. The interpolated velocities are 25.11 and − 18.30 mm/year for T102, 28.44 and − 19.77 mm/year for T103, and 9.79 and − 7.51 mm/year for T105 in the north and east directions, respectively (Table 2). Once the interseismic velocities were generated, we subtracted the velocities from the postseismic observations. As a result, the observations should only have the non-linear postseismic component. We then fitted the time series by the following equation.

$$y(t_i) = a + \sum_{1}^{n_k} k_j \cdot \log\left[1 + \left(t_i - t_{\mathrm{eq}}\right)/p\right] + \varepsilon \qquad (2)$$

Here, we only fitted the time series with the initial coordinate a and the logarithmic pattern. We ignored the seasonal variation because we cannot correctly estimate the

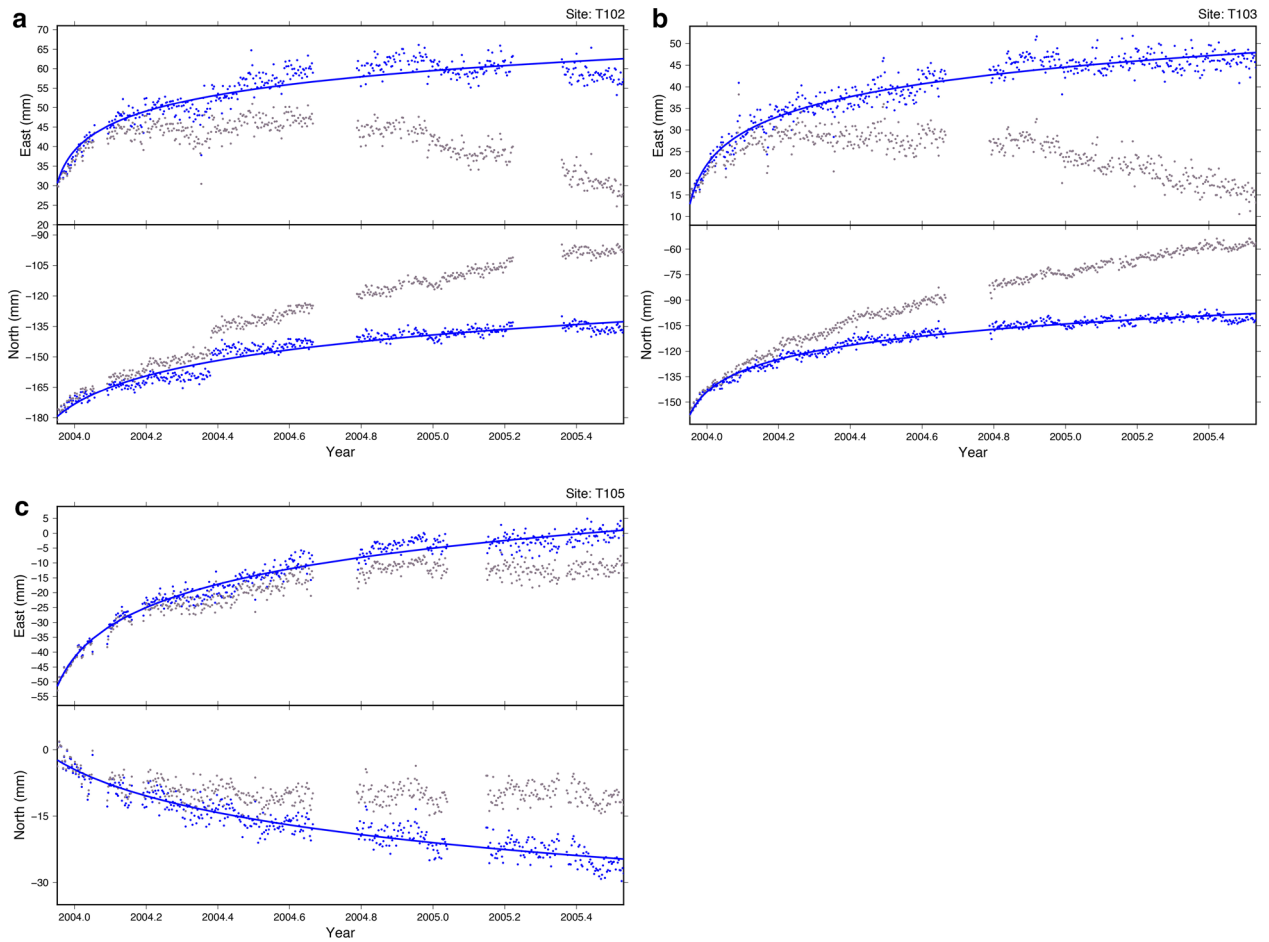

Fig. 4 Postseismic time series fitting for stations **a** T102, **b** T103 and **c** T105. Grey dots are original GPS time series, and blue dots are postseismic signals only with interseismic velocities removed. Blue lines are postseismic fitting using the logarithmic function

annual and semi-annual variations by spatial interpolation. Figure 4 shows the results of the logarithmic fitting for the three stations and the postseismic decay patterns can be characterized. All the results of time-series fitting for the stations with incomplete data are available in Additional file 2.

Postseismic grid model

As we estimated the logarithmic decay functions and interseismic velocities at all stations, we generated a postseismic deformation grid model for the maintenance of semi-kinematic reference frames. According to the GPS time series fitting, the surface deformation after the earthquake should contain at least interseismic velocities and postseismic decays. After properly estimating the linear interseismic velocity and non-linear postseismic decay at each GPS station, we are then able to predict the amount of surface displacements at a given time duration after the earthquake. Since we have the linear velocities derived from either time series fitting or spatial interpolation for interseismic deformation and logarithmic fitting curves for postseismic deformation, we can estimate the accumulative displacements for postseismic deformation and post-earthquake (postseismic + interseismic) deformation (data available in Additional file 3). Moreover, following the method of Ching and Chen (2015) and Li et al. (2019), we used the kriging interpolation to generate a grid model of postseismic deformation and post-earthquake deformation within a certain time period using the estimated interseismic and postseismic displacements at every continuously recorded GPS stations. Figure 5 shows the grid models of postseismic deformation and post-earthquake deformation with accumulative displacements in the period between the Chengkung and Taitung earthquakes. We conducted the grid models for the hanging wall and footwall areas separately and

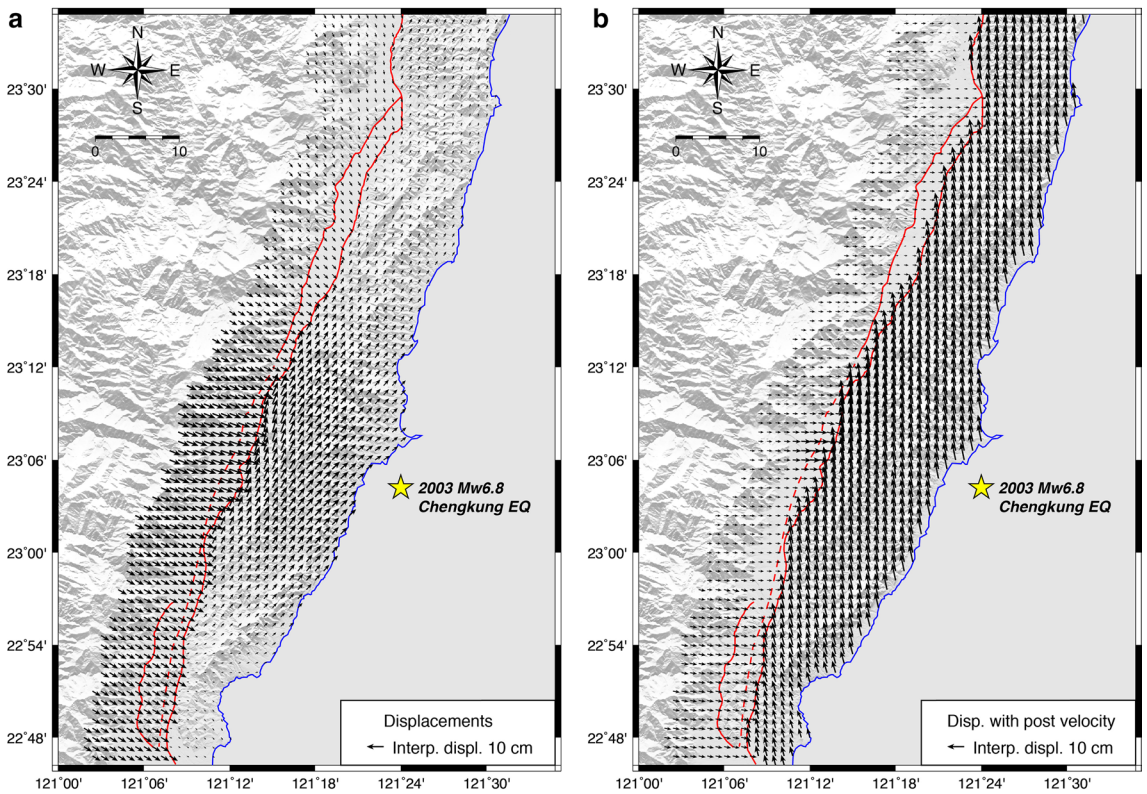

Fig. 5 Grid models of accumulative displacements for **a** only postseismic deformation and **b** total deformation including postseismic and interseismic movements. Time span of the accumulative displacements is from the 2003 Chengkung earthquake to 2006 Taitung earthquake. Yellow star denotes the epicenter of the Chengkung earthquake. Red lines are the active faults shown in Fig. 1. Figure 5a provides amount of postseismic displacements, which can be used to calculate how much postseismic deformation occurred. Figure 5b shows amount of total displacements after the earthquake, which can be used to justify if the total displacements exceed the tolerance of the reference frame

integrated the results together to generate regional grid models as shown in Fig. 5.

To validate the grid model, we used independent GPS observations within the study area. The grid model can be validated using other geodetic measurements or surface displacements derived from imaging geodesy. After searching for geodetic data, we found that two datasets of continuous and campaign GPS could be used for the validation. There are three continuous GPS stations in the area, which were not used to construct the grid model, including ERPN, LONT, and PING. These three stations were installed only a year before the Chengkung earthquake so we did not use their time series for our tests. Because the first two stations are located in the southernmost Longitudinal Valley within the fault zone of the southernmost Longitudinal Valley fault (Chuang et al. 2014), their deformation behaviors are complicated. Therefore, we chose to use the observations of PING, which is at least 10 km away from surrounding GPS stations, to validate our grid model (Fig. 1). We computed the total displacement at the station based on our grid model (Fig. 5b) and compared the interpolated displacement to the actual displacement derived from the time series. The result shows that the model displacements are −20.64 mm and 97.48 mm while the actual displacements are −17.89 mm and 77.20 mm in the east and north directions, respectively, for the time period of ~2 years after the Chengkung earthquake. The difference is well below the accuracy requirement of cadastral surveys of 60 mm. In addition, we used campaign GPS data of postseismic deformation (Chen et al. 2006), which was surveyed ~4 months after the earthquake, to validate our grid model. We computed a grid model of total displacements for 4 months and compared its result to the campaign data. The accuracy is 11.3 mm and 16.1 mm in the east and north directions, respectively. Through these two accuracy assessments, the accuracy of our grid models is generally below 20 mm, which fulfills the need of cadastral surveys. Further validation may be required using other geodetic observations or results derived from synthetic aperture radar (SAR) images (e.g., Champenois et al. 2012).

Usage of postseismic grid model to the semi-kinematic reference frame

We proposed the grid models for the postseismic deformation to correct the semi-kinematic reference frame in Taiwan. We created the grid model with the latitude and longitude spacing of 0.01°, which is similar to the baseline of fourth-order control points (original triangulation benchmarks) and cadastral benchmarks in Taiwan. Once the logarithmic patterns are estimated, one can easily estimate accumulative displacements at a specific time and generate the grid model by kriging interpolation. For practical usage, we demonstrated two types of grid models. One has postseismic displacements only (Fig. 5a), which provides the estimates of the excess postseismic displacements in addition to steady interseismic deformation. The other model has the accumulative displacements including interseismic and postseismic movements, which provide an immediate view to evaluate the total displacements after an earthquake.

Discussion

In this study, we explored approaches to accommodate the non-linear pattern of postseismic time series and to generate a deformation model for the maintenance of the semi-kinematic reference frame in Taiwan. The transient characteristics of postseismic deformation not only reflect the dynamic properties of seismogenic faults but also complicate the process to approximate GPS time series.

Following the idea of earthquake-cycle deformation and the convention of GPS time series fitting, we implemented the logarithmic function to fit the postseismic time series. Compared with the method of piecewise linear fitting, our method can fit the non-linear pattern with one single function. Since the 2003 Chengkung earthquake is dominated by afterslip, which is mostly the prominent mechanism for many seismic events especially for crustal faults, the logarithmic function can fit and predict the non-linear pattern well with early observations after the earthquake (Fig. 2). In addition, as no obvious poroelastic deformation of the earthquake, which is another postseismic deformation mechanism generally occurred shortly and near the fault (e.g., Peltzer et al. 1998), we do not need to exclude early observations (Bevis and Brown 2014) and the logarithmic function can work properly. Consequently, the logarithmic function can serve as a useful approximation for the postseismic deformation of the 2003 Chengkung earthquake. Considering the tectonic environment of a fault-and-thrust belt and active orogen, the island of Taiwan is subject to earthquake-related deformation on crustal faults (Shyu et al. 2005, 2016) and presumably it is reasonable to simply use the logarithmic function to accommodate non-linear postseismic deformation for earthquakes in the Taiwan area. In terms of the realization of semi-kinematic reference frames, such a logarithmic approximation can well predict the non-linear trend, providing useful information about the amount of postseismic displacements at a certain time period and helping to estimate the timing to correct the reference frame.

The method of GPS time series fitting with the functions analogous to earthquake-cycle deformation can provide a stable approximation of crustal movement even with incomplete time series. The idea of the time series fitting simply decomposes the observations into interseismic, coseismic and postseismic deformation approximated by linear, step and logarithmic functions, respectively. Although this method is technically a regression for time series data, it follows explainable geophysical mechanisms of fault behaviors. Together with the logarithmic function, the linear function for interseismic deformation can help stably fit postseismic deformation and provide simple velocity reference to determine whether the postseismic deformation is ceased. On the other hand, however, if GPS time series is incomplete, more specifically without observations before the earthquake, the interseismic linear function is not constrained, making the logarithmic fitting unstable. As the installation of continuously recorded GPS stations is conducted by different agencies resulting in nonuniform installation time, the observation periods of the GPS time series in Taiwan are commonly varied and often generate incomplete time series not to capture enough observations associated with interseismic, coseismic and postseismic deformation. Therefore, to better use data at continuous GPS stations with incomplete time series, we estimated interseismic velocities at the locations of those stations by spatial interpolation from surrounding stations with preseismic observations. With the constrained interseismic velocities, postseismic movements at the sites without preseismic observations can easily be approximated.

After the postseismic decays were properly estimated at all GPS sites, we proposed the postseismic deformation grid models to correct the reference frame. Following the ongoing architecture of the semi-kinematic reference frame of Taiwan, which proposed deformation models to correct interseismic deformation (Ching and Chen 2015) and coseismic displacements (Li et al. 2019), we constructed two grid models of accumulative postseismic displacements with given postseismic time period (Fig. 5) using the estimated logarithmic curves at the GPS sites. The two grid models estimate only postseismic deformation and total deformation after the earthquake. The first model with only postseismic deformation can provide clear sense of the amount of accumulative postseismic displacements, which is easier to locate

the area of postseismic deformation and track the postseismic decay. On the other hand, because afterslip might generate a similar displacement pattern with coseismic deformation, the total displacements may be canceled if the postseismic displacement direction is opposite to the interseismic displacements especially in the footwall area in this study (Fig. 5b), which consequently will extend the timing to correct the reference frame in such area. Therefore, the latter model with total post-earthquake (postseismic + interseismic) deformation is straightforward for users to determine whether they have to make the correction after an earthquake. Thus, the two proposed grid models can provide useful information to track postseismic deformation and to determine the timing to correct the reference frame in different ways.

In terms of maintaining the reference frame accuracy, it is crucial to characterize time-dependent information of surface deformation. If the information is well constrained, the time-dependent displacements can be used to update official coordinates and to access future deformation patterns. In previous work for examining the realization of the semi-kinematic reference frame in Taiwan, Ching and Chen (2015) explored the usage of interpolation and block models to characterize interseismic deformation, and Li et al. (2019) established a framework to integrate interpolation models for interseismic and coseismic deformation. In this study, we examined the approaches to use complete and incomplete time series to characterize non-linear postseismic deformation for the maintenance of the semi-kinematic reference frame. Once we estimate the amount of postseismic displacements as described above, we can plan and control the timing for updating the reference frame. By incorporating the fitting of non-linear postseismic deformation, we considered all the components of a full earthquake cycle (interseismic, coseismic and postseismic deformation), which could appropriately describe time-dependent displacements. The current examination of the Taiwan semi-kinematic reference frame including this and previous studies (Ching and Chen 2015; Li et al. 2019) focuses on the horizontal component. The realization of the full 3D reference frame will be one future task, and the validation and comparison of the reference frame using other geodetic data are also important for future work.

Conclusion

We explored the methods to implement a non-linear postseismic deformation model for the Taiwan semi-kinematic reference frame using the 2003 Chengkung earthquake as an example. We adopted a logarithmic function in response to the afterslip-dominant postseismic deformation of the Chengkung earthquake to approximate the non-linear postseismic decays at continuous GPS sites. Following the concept of earthquake-cycle deformation, we fitted the GPS observations with linear, step, and logarithmic functions for the complete time series. For the time series without preseismic observations, we subtracted the interseismic velocities by spatial interpolation from the incomplete time series and fitted the resultant time series with the logarithmic function. After properly estimating postseismic decays at all GPS sites, we conducted two grid models for accumulative postseismic displacements. The first grid model can clearly track postseismic movements, and the latter model can access the total amount of surface displacements. The implementation of the grid models can provide useful prediction for tracking surface movements to access the timing and amount of displacements to correct the semi-kinematic reference frame (Additional files 1, 2, 3).

Supplementary information

Supplementary information accompanies this paper at https://doi.org/10.1186/s40623-020-01209-y.

Additional file 1. GPS time-series fitting results for the stations with preseismic data.

Additional file 2. GPS time-series fitting results for the stations without preseismic data.

Additional file 3. Accumulative displacements of the GPS stations to construct grid models in this study.

Abbreviations

TWD97: Taiwan geodetic datum 1997; GPS: Global Positioning System; ITRF94: International Terrestrial Reference Frame 1994; ITRF2008: International Terrestrial Reference Frame 2008; RMS: Root mean square; GNSS: Global Navigation Satellite System; SAR: Synthetic aperture radar.

Acknowledgements

We thank the Central Weather Bureau, Ministry of Interior, National Land Surveying and Mapping Center, Central Geological Survey, Institute of Earth Sciences, and National Taiwan University for providing data. Figures were generated using the Generic Mapping Tools (GMT), developed by Wessel et al. (2013).

Authors' contributions

Both Kwo-Hwa Chen and Ray Y. Chuang initiated the study and forming the conceptual ideas. Kwo-Hwa Chen conducted the collection, processing and analysis of data and paper writing. Ray Y. Chuang and Kuo-En Ching helped paper writing and result verification. All authors read and approved the final manuscript.

Funding

This research is supported by the Ministry of Science and Technology with project number of 107-2221-E-305-008-MY3 and 107-2116-M-002-021-MY2.

Availability of data and materials

The GPS time series used in this study is adopted from the GPS lab of the Taiwan Earthquake Center (http://gps.earth.sinica.edu.tw). The dataset supporting the conclusions of this article is included within the article and additional files.

Ethics approval and consent to participate

Not applicable.

Consent for publication
Not applicable.

Competing interests
All the authors do not have any financial competing interests. None of the authors of this manuscript held any stocks, shares, and patents related to the content.

Author details
[1] Department of Real Estate and Built Environment, National Taipei University, New Taipei City 23741, Taiwan. [2] Department of Geography, National Taiwan University, Taipei 10617, Taiwan. [3] NTU Research Center for Future Earth, Taipei 10617, Taiwan. [4] Department of Geomatics, National Cheng Kung University, Tainan 70101, Taiwan.

Received: 3 March 2020 Accepted: 24 May 2020
Published online: 01 June 2020

References

Altamimi Z, Collilieux X, Legrand J, Garayt B, Boucher C (2007) ITRF2005: a New Release of the International Terrestrial Reference Frame based on time series of station positions and Earth Orientation Parameters. J Geophys Res 112:B09401. https://doi.org/10.1029/2007JB004949

Altamimi Z, Collilieux X, Métivier L (2011) ITRF2008: an improved solution of the International Terrestrial Reference Frame. J Geod 85(8):457–473. https://doi.org/10.1007/s00190-011-0444-4

Altamimi Z, Rebischung P, Metivier L, Collilieux X (2016) ITRF2014: a new release of the International Terrestrial Reference Frame modeling nonlinear station motions. J Geophys Res 121:6109–6131. https://doi.org/10.1002/2016JB013098

Bevis M, Brown A (2014) Trajectory models and reference frames for crustal motion geodesy. J Geod 88(3):283–311. https://doi.org/10.1007/s00190-013-0685-5

Blick G, Donnelly N (2016) From static to dynamic datums: 150 years of geodetic datums in New Zealand. N Z J Geol and Geophys 59(1):15–21. https://doi.org/10.1080/00288306.2015.1128451

Blick G, Crook C, Grant D, Beavan J (2003) Implementation of a semi-dynamic datum for New Zealand. Int Assoc Geod Symposia 128:38–43. https://doi.org/10.1007/3-540-27432-4_7

Byrne T, Chan YC, Rau RJ, Lu CY, Lee YH, Wang YJ (2011) The arc-continent collision in Taiwan. In: Brown D, Ryan PD editor. Arc-continent collision. pp 213–246. https://doi.org/10.1007/978-3-540-8858-0_8

Champenois J, Fruneau B, Pathier E, Deffontaines B, Lin KC, Hu JC (2012) Monitoring of active tectonic deformations in the Longitudinal Valley (Eastern Taiwan) using Persistent Scatterer InSAR method with ALOS PALSAR data. Earth Planet Sci Lett 337–338:144–155. https://doi.org/10.1016/j.epsl.2012.05.025

Chang WL, Ching KE, Lee CH, Lee YR, Lee CF (2016) Earthquake potential of active faults in Taiwan from GPS observations and block modeling. Seismo Res Lett 87(6):1274–1286. https://doi.org/10.1785/0220160094

Chen HY, Yu SB, Kuo LC, Liu CC (2006) Coseismic and postseismic surface displacements of the 10 December 2003 (*Mw* 6.5) Chengkung, eastern Taiwan, earthquake. Earth Planet Space 58:5–21. https://doi.org/10.1186/BF03351908

Cheng LW, Lee JC, Hu JC, Chen HY (2009) Coseismic and postseismic slip distribution of the 2003 Mw = 6.5 Chengkung earthqauke in eastern Taiwan: Elastic modeling from inversion of GPS data. Tectonophysics 466(3–4):335–343. https://doi.org/10.1016/j.tecto.2007.11.021

Ching KE, Chen KH (2015) Tectonic effect for establishing a semi-dynamic datum in Southwest Taiwan. Earth Planets Space 67:207. https://doi.org/10.1186/s40623-015-0374-0

Ching KE, Rau RJ, Zeng Y (2007) Coseismic source model of the 2003 M_w 6.8 Chengkung earthquake, Taiwan, determined from GPS measurements. J Geophys Res 112:B06422. https://doi.org/10.1029/2006JB004439

Ching KE, Rau RJ, Johnson KM, Lee JC, Hu JC (2011) Present-day kinematics of active mountain building in Taiwan from GPS observations during 1995–2005. J Geophys Res 116:B09405. https://doi.org/10.1029/2010JB008058

Chuang RY, Miller MM, Chen YG, Chen HY, Shyu JBH, Yu SB, Rubin CM, Sieh K, Chung LH (2012) Interseismic deformation and earthquake hazard along the southernmost Longitudinal Valley fault, eastern Taiwan. Bull Seismol Soc Am 102(4):1569–1582. https://doi.org/10.1785/0120110262

Chuang RY, Johnson KM, Kuo YT, Wu YM, Chang CH, Kuo LC (2014) Active back thrust in the eastern Taiwan suture revealed by the 2013 Rueisuei earthquake: evidence for a doubly vergent orogenic wedge? Geophys Res Lett 41(10):3464–3470. https://doi.org/10.1002/2014GL060097

Crook C, Donnelly N, Beavan J, Pearson C (2016) From geophysics to geodetic datum: updating the NZGD2000 deformation model. N Z J Geol and Geophys 59(1):22–32. https://doi.org/10.1080/00288306.2015.1100641

Freed AM, Bürgmann R, Calais E, Freymueller J, Hreinsdóttir S (2006) Implications of deformation following the 2002 Denali, Alaska, earthquake for postseismic relaxation processes and lithospheric rheology. J Geophys Res 111:B01401. https://doi.org/10.1029/2005JB003894

Hearn E (2003) What can GPS data tell us about the dynamics of post-seismic deformation? Geophys J Int 155:753–777. https://doi.org/10.1111/j.1365-246X.2003.02030.x

Hetland EA, Hager BH (2006) The effects of rheological layering on postseismic deformation. Geophys J Int 166:277–292. https://doi.org/10.1111/j.1365-246X.2006.02974.x

Hsu L, Bürgmann R (2006) Surface creep along the Longitudinal Valley fault, Taiwan from InSAR measurements. Geophys Res Lett 33:L06312. https://doi.org/10.1029/2005GL024624

Hsu YJ, Yu SB, Chen HY (2009a) Coseismic and postseismic deformation associated with the 2003 Chengkung, Taiwan, earthquake. Geophys J Int 176(2):420–430. https://doi.org/10.1111/j.1365-246X.2008.04009.x

Hsu YJ, Yu SB, Simons M, Kuo LC, Chen HY (2009b) Interseismic crustal deformation in the Taiwan plate boundary zone revealed by GPS observations, seismicity, and earthquake focal mechanisms. Tectonophysics 479:4–18. https://doi.org/10.1016/j.tecto.2008.11.016

Klein E, Bock Y, Xu X, Sandwell DT, Golriz D, Fang P, Su L (2019) Transient deformation in California from two decades of GPS displacements: implications for a three-dimensional kinematic reference frame. J Geophys Res 124:12189–12223. https://doi.org/10.1029/2018JB017201

Kuochen H, Wu YM, Chen YG, Chen RY (2007) 2003 Mw6.8 Chengkung earthquake and its related seismogenic structures. J Asian Earth Sci 31(3):332–339. https://doi.org/10.1016/j.jseaes.2006.07.028

Lee JC, Angelier J, Chu HT, Jeng FS (2001) Continuous monitoring of an active fault in a plate suture zone: a creepmeter study of the Chihshang Fault, eastern Taiwan. Tectonophysics 333(1–2):219–240. https://doi.org/10.1016/S0040-1951(00)00276-6

Lee JC, Angelier J, Chu HT, Hu JC, Jeng FS, Rau RJ (2003) Active fault creep variations at Chihshang, Taiwan, revealed by creep meter monitoring, 1998–2001. J Geophys Res 108(B11):2528. https://doi.org/10.1029/2003JB002394

Li CK, Ching KE, Chen KW (2019) The ongoing modernization of the Taiwan semi-dynamic datum based on the surface horizontal deformation model using GNSS data from 2000 to 2016. J Geod 93:1543–1558. https://doi.org/10.1007/s00190-019-01267-5

Lin KC, Hu JC, Ching KE, Angelier J, Rau RJ, Yu SB, Tsai CH, Shin TC, Huang MH (2010) GPS crustal deformation, strain rate, and seismic activity after the 1999 Chi-Chi earthquake in Taiwan. J Geophys Res 115:B07404. https://doi.org/10.1029/2009JB006417

Marone CJ, Scholtz CH, Bilham R (1991) On the mechanics of earthquake afterslip. J Geophys Res 96(B5):8441–8452. https://doi.org/10.1029/91JB00275

McCaffrey R (2005) Block kinematics of the Pacific–North America plate boundary in the southwestern United States from inversion of GPS, seismological, and geologic data. J Geophys Res 110:B07401. https://doi.org/10.1029/2004JB003307

Meade BJ, Hager BH (2005) Block model of crustal motion in southern California constrained by GPS measurements. J Geophys Res 110:B03403. https://doi.org/10.1029/2004JB003209

Nikolaidis R (2002) Observation of geodetic and seismic deformation with the Global Positioning System. Dissertation, University of California, San Diego

Nur A, Mavko G (1974) Post-seismic viscoelastic rebound. Science 183:204–206. https://doi.org/10.1126/science.183.4121.204

Pearson C, Snay R (2012) Introducing HTDP 3.1 to transform coordinates across time and spatial reference frames. GPS Solut 17(1):1–15. https://doi.org/10.1007/s10291-012-0255-y

Pearson C, McCaffrey R, Elliott J, Snay R (2010) HTDP 3.0: software for coping with the coordinate changes associated with crustal motion. J Surv Eng 136:80–90. https://doi.org/10.1061/(ASCE)SU.1943-5428.0000013
Peltzer G, Rosen P, Rogez F, Hudnut K (1998) Poroelastic rebound along the Landers 1992 earthquake surface rupture. J Geophys Res 103:30131–30145. https://doi.org/10.1029/98JB02302
Perfettini H, Avouac JP (2004) Postseismic relaxation driven by brittle creep: a possible mechanism to reconcile geodetic measurements and the decay rate of aftershocks, application to the Chi-Chi earthquake, Taiwan. J Geophys Res 109:B02304. https://doi.org/10.1029/2003JB002488
Pollitz FF (1997) Gravitational viscoelastic postseismic relaxation on a layered spherical Earth. J Geophys Res 102(B8):17921–17941. https://doi.org/10.1029/97JB01277
Savage JC, Svarc JL (1997) Postseismic deformation associated with the 1992 $M_w = 7.3$ Landers earthquake, southern California. J Geophys Res 102:7565–7577. https://doi.org/10.1029/97JB00210
Savage JC, Yu SB (2007) Postearthquake relaxation and aftershock accumulation linearly related after the 2003 *M* 6.5 Chengkung, Taiwan, and the 2004 *M* 6.0 Parkfield, California, earthquakes. Bull Seismol Soc Am 97:1632–1645. https://doi.org/10.1785/0120070069
Savage JC, Svarc JL, Yu SB (2005) Postseismic relaxation and transient creep. J Geophys Res 110:B11402. https://doi.org/10.1029/2005JB003687
Scholz CH (1998) Earthquake and friction laws. Nature 391:37–42. https://doi.org/10.1038/34097
Shen ZK, Jackson DD, Feng Y, Cline M, Kim M, Fang P, Bock Y (1994) Postseismic deformation following the Landers earthquake, California, 28 June 1992. Bull Seismol Soc Am 84(3):780–791
Shyu JBH, Sieh K, Chen YG, Liu CS (2005) Neotectonic architecture of Taiwan and its implications for future large earthquakes. J Geophys Res 110:B08402. https://doi.org/10.1029/2004JB003251
Shyu JBH, Sieh K, Chen YG, Chung LH (2006) Geomorphic analysis of the Central Range fault, the second major active structure of the Longitudinal Valley suture, eastern Taiwan. GSA Bull 118(11–12):1447–1462. https://doi.org/10.1130/B25905.1
Shyu JBH, Chung LH, Chen YG, Lee JC, Sieh K (2007) Re-evaluation of the surface ruptures of the November 1951 earthquake series in eastern Taiwan, and its neotectonic implications. J Asian Earth Sci 31(3):317–331. https://doi.org/10.1016/j.seaes.2006.07.018
Shyu JBH, Sieh K, Chen YG, Chuang RY, Wang Y, Chung LH (2008) Geomorphology of the southernmost Longitudinal Valley fault: Implications for evolution of the active suture of eastern Taiwan. Tectonics 27(1):TC1019. https://doi.org/10.1029/2006TC002060
Shyu JBH, Chuang YR, Chen YL, Lee YR, Cheng CT (2016) A new on-land seismogenic structure source database from the Taiwan Earthquake Model (TEM) project for seismic hazard analysis of Taiwan. Terr Atmos Ocean Sci 27(3):311–323. https://doi.org/10.3319/TAO.2015.11.27.02
Suppe J (1981) Mechanics of mountain building and metamorphism in Taiwan. Mem Geol Soc China 4:67–89
Suppe J (1984) Kinematics of arc-continent collision, flipping of subduction, and back-arc spreading near Taiwan. Mem Geol Soc China 6:21–33
Tanaka Y, Saita H, Sugawara J, Iwata K, Toyoda T, Hirai H, Kawaguchi T, Matsuzaka S (2007) Efficient maintenance of the Japanese geodetic datum 2000 using crustal deformation models—PatchJGD & semi-dynamic datum. Bull Geogr Surv Inst 54:49–59
Teng LS (1990) Geotectonic evolution of late Cenozoic arc-continent collision in Taiwan. Tectonophysics 183:57–76. https://doi.org/10.1016/0040-1951(90)90188-E
Tobita M (2016) Combined logarithmic and exponential function model for fitting postseismic GNSS time series after 2011 Tohoku-Oki earthquake. Earth Planets Space 68:41. https://doi.org/10.1186/s40623-016-0422-4
Wessel P, Smith WHF, Scharroo R, Luis J, Wobbe F (2013) Generic Mapping Tools: improved version released. Eos 94(45):409–410. https://doi.org/10.1002/2013EO450001
Wu YM, Chen YG, Shin TC, Kuochen H, Hou CS, Hu JC, Chang CH, Wu CF, Teng TL (2006a) Coseismic versus interseismic ground deformations, fault rupture inversion and segmentation revealed by 2003 *Mw* 6.8 Chengkung earthquake in eastern Taiwan. Geophys Res Lett 33:L02312. https://doi.org/10.1029/2005GL024711
Wu YM, Chen YG, Chang CH, Chung LH, Teng TL, Wu FT, Wu CF (2006b) Seismogenic structure in a tectonic suture zone: With new constraints from 2006 Mw6.1 Taitung earthquake. Geophys Res Lett 33(22):L22305. https://doi.org/10.1029/2006GL027572
Wu YM, Chang CH, Zhao L, Teng TL, Nakamura M (2008) A comprehensive relocation of earthquakes in Taiwan from 1991 to 2005. Bull Seismol Soc Am 98(3):1471–1481. https://doi.org/10.1785/0120070166
Yang M, Tseng CL, Yu JY (2001) Establishment and maintenance of Taiwan geodetic datum 1997. J Surv Eng 127(4):119–132. https://doi.org/10.1061/(ASCE)0733-9453(2001)127:4(119)
Yu SB, Kuo LC (2001) Present-day crustal motion along the Longitudinal Valley Fault, eastern Taiwan. Tectonophysics 333(1–2):199–217. https://doi.org/10.1016/S0040-1951(00)00275-4
Yu SB, Chen HY, Kuo LC (1997) Velocity field of GPS stations in the Taiwan area. Tectonophysics 274:41–59. https://doi.org/10.1016/S0040-1951(96)00297-1

Publisher's Note